Cortez, L. E., & Ito, E. (2025), Hazard assessment through site characterization and strong motion simulation toward disaster mitigation in Acajutla, El Salvador. Synopsis of IISEE-GRIPS Master's Thesis, Bulletin of IISEE, 60

HAZARD ASSESSMENT THROUGH SITE CHARACTERIZATION AND STRONG MOTION SIMULATION TOWARD DISASTER MITIGATION IN ACAJUTLA, EL SALVADOR

Luis Eduardo CORTEZ HERNÁNDEZ[1] **Supervisor: Eri ITO**[2]

ABSTRACT

Despite being in a seismically active region, the city of Acajutla lacks quantitative seismic hazard assessments. This study aims to evaluate local seismic hazards through site characterization using microtremor observations. The Earthquake-to-Microtremor Ratio (EMR) method from observed seismic and microtremor ground motions was applied to transform the horizontal-to-vertical spectral ratios of microtremors (MHVRs) into pseudo-horizontal-to-vertical spectral ratios of earthquakes (pEHVRs), which were used to derive shear-wave velocity models at all microtremor observation sites (32 in total) around the Port of Acajutla. Based on these models, site amplification factors were computed, and strong ground motions were estimated. The MHVR results indicate a consistent sag in amplitude near 1 Hz, suggesting unique geological conditions in the deeper layers of the subsurface, namely a high P-wave velocity contrast at a depth of approximately 500 m. This interpretation was reinforced by the velocity models obtained through inversion, as a manifestation of the significant amplification observed only in the vertical component. Furthermore, the estimated strong ground motions imply that the seismic responses across the study area would be rather uniform, even in the event of a future megathrust earthquake. This finding suggests that Acajutla is relatively safe in terms of the general characteristics of its site effects. The aforementioned discovery of unique geological conditions is indirectly supported by the existence of similar sites in the Japanese strong-motion networks (K-NET and KiK-net). This study represents the first detailed and quantitative evaluation of local site effects in this city and provides valuable insights for future seismic hazard assessments in the region.

Keywords: Microtremors, Site Effects, Seismic Hazard, Ground Motion.

1. INTRODUCTION

El Salvador, with an area of 21,040 km², is in a tectonically active zone due to the interaction of the Cocos, Caribbean, and North American plates (Guzmán‐Speziale et al., 1989). The oblique subduction of the Cocos Plate beneath the Caribbean Plate, at 65–75 mm/yr (DeMets et al., 2010), generates earthquakes along the Wadati–Benioff zone and forms the Central American Volcanic Arc (Bommer et al., 2002; Canora et al., 2010). Seismicity occurs both at the subduction interface and within the slab, producing shallow and intermediate-depth earthquakes such as those in 2001 (Bommer et al., 2002). Additionally, forearc deformation produces active faults in the El Salvador Fault Zone (Martínez-Díaz et al., 2021).

The target area of this study is Acajutla, a city located in the western part of El Salvador that directly borders the Pacific Ocean. It is home to El Salvador's main international seaport: the Port of Acajutla. Additionally, it is home to oil refineries and natural gas plants, making it a strategic point

[1] University of El Salvador (UES), El Salvador.
[2] International Institute of Seismology and Earthquake Engineering, Building Research Institute.

Approved as Master Paper of DMP by BRI/GRIPS

for the Salvadoran economy and development. Overall, 15 tsunamis were recorded in El Salvador between 1859 and 2012, and at least two of them were recorded in the Acajutla area (Fernández A, 2011; Álvarez-Gómez et al., 2013). Despite its susceptibility to seismic activity, there is limited information regarding actual seismic hazards, and no studies have assessed how local ground conditions amplify earthquake shaking, which is crucial for a quantitative understanding of seismic hazards. This lack of data is of particular concern due to the region's tectonic settings. In order to address this gap, the objective of the study is to conduct a hazard assessment through site characterization and strong motion simulation, based on observation of microtremor data, and applying the Earthquake-to-Microtremor Ratio (EMR) method proposed by Kawase et al. (2018) to obtain the velocity structures.

2. DATA

Microtremor observations were conducted between May 4 and May 8, 2025, in 32 sites distributed in the urban center of Acajutla, using a two McSEIS-AT three-channel microtremor exploration system manufactured by OYO Corporation. Measurement sites were distributed throughout the city at regular intervals of approximately 500 m, as shown in Figure 1. Each recording lasted around 30 minutes under stable weather conditions. In addition to the microtremor measurements, seismic event records were obtained from a permanent accelerometric station, equipped with a Wilmot SR-100 seismograph, located at site SS-1 (Figure 1). The recorded events were used in this study to calculate the Earthquake Horizontal-to-Vertical Spectral Ratio (EHVR). Seismic events were selected to ensure reliable EHVR analysis, including only those with PGA ≤ 200 gal, focal depths ≤ 60 km, Mw > 4.5, and epicentral distances ≤ 200 km. Based on these criteria, a total of 10 events were selected. The Ministry of Environment and Natural Resources (MARN) provided the waveform data, which included the three components necessary for EHVR computation.

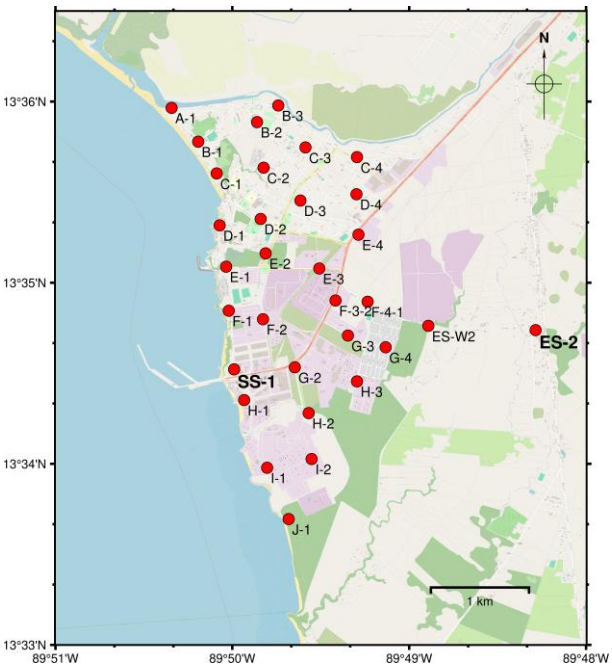

Figure 1. Distribution map of microtremor observations shown in red circles. The base map was generated using OpenStreetMap data.

We used a down-hole Vs profile from ES-2 (Figure 1) for the inversion, obtained during a MARN groundwater monitoring project in 2019. The 50 m survey, sampled at 1 m intervals, showed Vs values from 137.3 m/s at the surface to 1063.4 m/s at depth, with a strong contrast between the first two layers and a gradual mid-depth decrease. This profile served as the basis for the new reference model applied in the inversion.

3. METHODOLOGY

3.1. MHVR

Microtremors are low-amplitude vibrations from natural and human sources (e.g., wind, sea waves, traffic, or machinery). Their observation is noninvasive, low-cost, and effective in areas with scarce seismic data. Nakamura (1989) suggested that MHVR could represent the S-wave resonant characteristics of the ground. However, the majority of the investigations showed that only the fundamental frequency is retrieved. Sánchez-Sesma et al. (2011) provided a theoretical basis within the diffuse field concept (DFC), relating MHVR to the square root of the ratio between the imaginary parts

of the horizontal and vertical components of the Green's function at the surface. In this study, MHVR was calculated from microtremor records following the procedure in Kawase et al. (2018): (1) dividing recordings into 40.96 s segments with 50% overlap, (2) selecting the 25% with the lowest noise, (3) computing Fourier spectra for NS, EW, and UD components with a 0.1 Hz Parzen window, (4) calculating NS/UD and EW/UD ratios, and (5) obtaining the RMS of both ratios. These MHVR results were later transformed via the EMR method into the pseudo EHVR (pEHVR). Thanks to this transformation, we can use the velocity inversion scheme based on the EHVR within the DFC framework for incident body waves (Kawase et al., 2011), where EHVR is essentially the ratio of S-wave to P-wave amplification from the seismological bedrock.

3.2. MHVR-to-pEHVR using EMR Method

Kawase et al. (2018) proposed the empirically derived EMR method to transform the MHVR into a pEHVR that shares similar characteristics to the EHVR. This reduces MHVR's limitations, lessens the need for large earthquake datasets, and enables efficient velocity inversion using only microtremor observations. For Acajutla, we constructed an EMR by dividing the EHVR obtained at the seismic station SS-1 by the MHVR at the same site (Eq. 1). The pEHVR at any other site was then obtained by multiplying Acajutla's EMR by the local MHVR (Eq. 2).

$$EMR_{Acajutla} = \frac{EHVR_{SS-1}}{MHVR_{SS-1}}, \tag{1}$$

$$pEHVR = EMR_{Acajutla} \times MHVR. \tag{2}$$

The EHVR at SS-1 was calculated using seismic records from the S-wave onset over a 40.96 s window. Fourier spectra for NS, EW, and UD components were computed via FFT, and NS/UD and EW/UD ratios were obtained. EHVR was defined as the RMS of both ratios, with no significant NS–EW differences, indicating no relevant 2D/3D effects (Matsushima et al., 2014). The final EHVR curve was the geometric average of all selected seismic events.

3.3. Inversion of Velocity Structure

The EHVR at SS-1 and the pEHVR at other sites were inverted using the same theoretical framework for EHVR. The method follows Nagashima et al. (2014, 2017), based on diffuse field theory and implemented through the Hybrid Heuristic Search method (Yamanaka, 2007), which combines Genetic Algorithms and Simulated Annealing to find a 1D layered subsurface model that best fits the observed H/V curves. A reference model was defined to set the search range, and 10 inversion runs of 200 generations each were performed, selecting the model with the minimum residual between observed and theoretical EHVR. Although the method can operate without a reference model, one was used here to avoid unrealistic solutions. The initial model, derived from boring data at ES-2, was adjusted to ensure layer continuity, gradual velocity increases, and representation of the seismological bedrock (Vs ≥ 3.2 km/s), where site amplification effects are negligible (Kawase et al., 2011). However, this model could not reproduce the sags in the lower-frequency range of the observed pEHVR, so a new reference model was constructed using the ES-2 velocity range and a trial-and-error approach (detailed in section 4.3).

3.4. Deconvolution and Convolution Analysis for Time History Estimates

Using the 1D velocity structures, deconvolution was performed at SS-1 by dividing the observed Fourier spectra by the horizontal and vertical site amplification factors (HSAF and VSAF), yielding bedrock spectral amplitudes. Applying the inverse Fourier transform with the observed phase, bedrock acceleration time histories were reconstructed. Convolution was then applied at each site by multiplying the bedrock spectra with the local HSAF and VSAF to obtain target site spectra. These were converted

into acceleration time histories through inverse Fourier transforms, again using the phase information from SS-1.

4. RESULTS

4.1. MHVR

We calculated MHVR for 32 sites from microtremor recordings, identifying the fundamental frequency and spectral characteristics of each. Most sites showed high fundamental frequencies with large amplitudes, indicating stiff ground. A common feature was a sag between 1–3 Hz, where the vertical component exceeded the horizontal in spectral amplitude (Figure 2). This suggests a weak S-wave impedance contrast with gradual velocity increase with depth and a stronger P-wave velocity contrast due to an abrupt structural change.

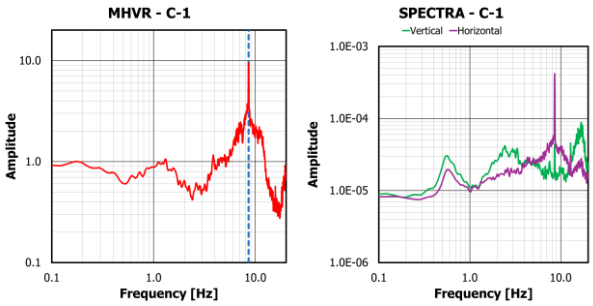

Figure 2. In the left figure, an example of MHVR for one site (in red), the dotted blue line indicates the fundamental peak frequency. In the right figure, the individual spectra for each component show the difference between the vertical (green) and horizontal (purple) components.

4.2. EMR for Acajutla and pEHVR

We constructed an EMR for Acajutla using the MHVR and EHVR at SS-1. As shown in Figure 3, MHVR and EHVR share a similar shape from 0.3 to 8.0 Hz. Above 8.0 Hz, MHVR becomes larger than EHVR, and subsequently EMR becomes less than 1.0. This EMR was used to transform the MHVR data into pEHVR data at all the observed sites. It is hardly idealistic to use this localized EMR calculated only from one site; however, MHVRs at other target sites share the same characteristics as the MHVR at SS-1 in the high-frequency band; therefore, the localized EMR should make MHVRs at other target sites similar to the EHVR at SS-1. It is notable how the sag observed in the MHVR is also retrieved in the pEHVR.

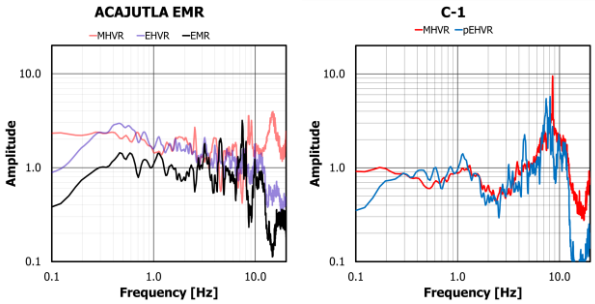

Figure 3. In the left figure, the comparison between MHVR (red) and EHVR (blue) at SS-1, and the EMR (black) is shown. In the right figure, a comparison between the MHVR (red) and pEHVR (blue) for the C-1 site.

4.3. Inversion Process for Velocity Structure

The inversion at SS-1, using the EHVR and the ES-2-based reference model, produced a realistic velocity profile with good agreement between the theoretical EHVR and the observed pEHVR. Then, we applied this model as a reference for other sites, but the results were unsatisfactory, with theoretical EHVRs deviating significantly from the observed pEHVRs and yielding unrealistic structures (e.g., >7 km sediment layers or excessively soft layers over bedrock). To address this, we develop a new reference model aiming at ES-2 through a trial-and-error approach, focusing on reproducing the sags observed in MHVR and

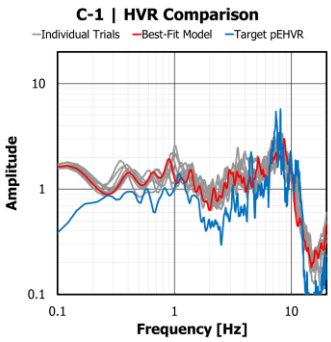

Figure 4. Comparison of HVR between the best-fit theoretical EHVR model (red) and the target pEHVR (blue). The gray line indicates the individual inversion trials.

pEHVR curves between 1–3 Hz. This model, with controlled searching ranges for Vs and Vp, was applied to all sites. While sag reproduction improved, amplitudes remained higher than observed due to the inversion program's emphasis on matching peaks in EHVR. Final models show significant P-wave impedance contrasts, while the S-wave velocity of the deep layers above the seismological bedrock is high, with a large thickness. (Figures 4 and 5).

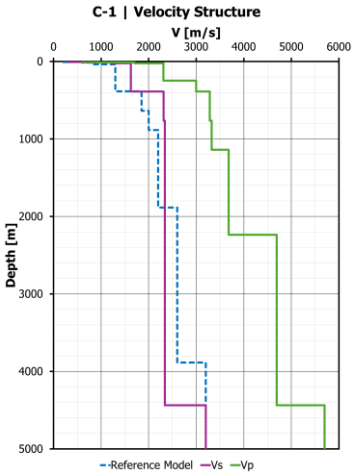

Figure 5. The inversion results show the velocity structure at the C-1 site, with the dotted blue line representing the reference model, the purple line for Vs, and the green line for Vp.

4.4. Distribution of HSAF and VSAF

Theoretical HSAF and VSAF were computed from the inverted velocity structures using one-dimensional multiple reflection theory. HSAF peak frequencies, mostly in the high-frequency range, indicate complex spatial variations in the shallow structure, while similarities at lower frequencies suggest a common deeper layer across the area, consistent with inversion results. VSAF peaks occur mainly at low frequencies with amplitudes larger than the typical value of ~2 at 1 Hz (Ito et al., 2020), corresponding to the sag in low-frequency MHVR. At some sites (e.g., SS-1, A-1 to C-1), we have higher peak frequencies due to resonance by the shallow layers (Figure 6).

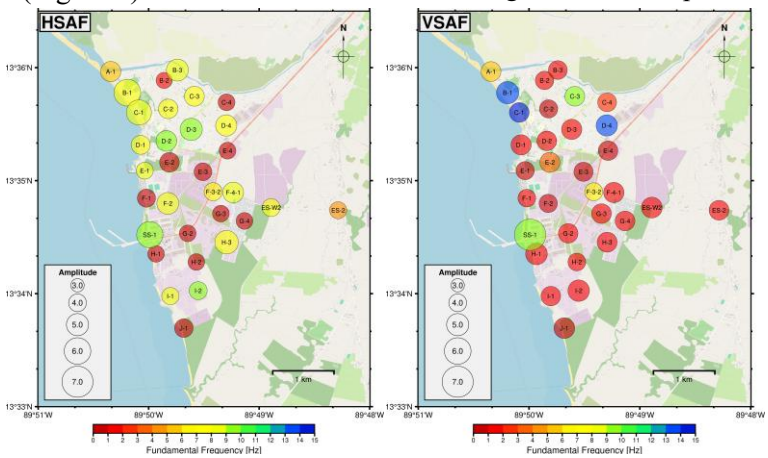

Figure 6. Distribution map of HSAF and VSAF, showing peak frequency by color and amplitude by circle size. Base map created with OpenStreetMap data.

4.5. Strong Ground Motion Estimation

Analysis of the January 13, 2001 (Mw 7.7) earthquake showed that PGA values at most sites were slightly lower than at SS-1 (Figure 7). Horizontal PGA ranged from 90–110 gal, with higher values (e.g., C-1, D-4, H-3) linked to slower S-wave velocities in the upper layers. Vertical PGA varied between 37–46 gal. The spatial differences were marginal, suggesting limited variation in site amplification across the area. SS-1 consistently showed the highest PGA, and if a similar megathrust event occurs in the future, stronger motion would be expected there. Combined with the inversion results, the findings indicate that nonlinearity effects could be negligible, and the area is relatively safe regarding site amplification, suggesting the importance of future studies on source, path, and building characteristics.

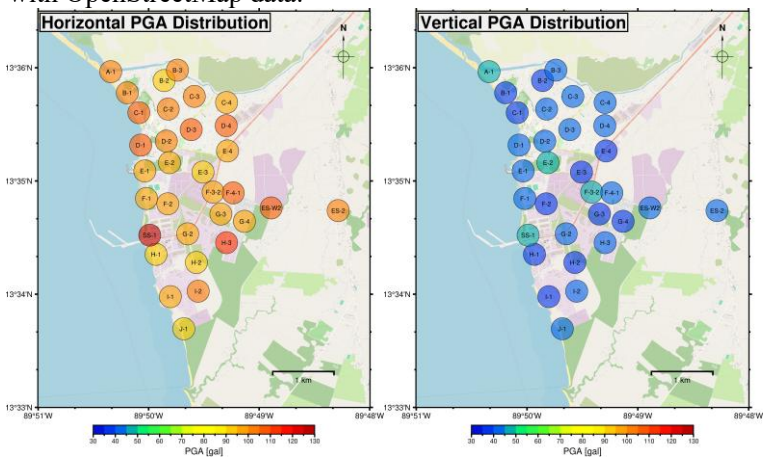

Figure 7. Distribution map of PGA in the horizontal and vertical components. The color scale indicates the value of PGA in gal. The base map was generated using OpenStreetMap data.

5. CONCLUSIONS

In this study, MHVR from microtremor observations in

Acajutla were transformed into pEHVR using the EMR derived from earthquake and microtremor data at the seismic station (SS-1). Most MHVR and pEHVR curves show a consistent sag between 1.0 and 3.0 Hz, linked to peaks in the vertical component, indicating particular geological conditions. The pEHVRs were used to invert subsurface velocity models, which explain the observed spectral characteristics and reveal distinct layer configurations. These models were then used to compute theoretical HSAF and VSAF to simulate seismic responses using the January 13, 2001, Mw 7.7 earthquake as a representative case. The simulations indicate that the strongest motions would occur at SS-1, where the HSAF is larger than other sites. This detailed site-effect study in Acajutla integrates pEHVR analysis, velocity inversion, and strong-motion simulation for the first time. Results show that, unlike typical soft-sediment basins in Japanese ports, Acajutla's subsurface structure is relatively stiff, offering favorable conditions for seismic disaster mitigation. The study provides a solid basis for future strong ground motion estimations in the area from any predicted bedrock motions.

ACKNOWLEDGEMENTS

I would like to express my heartfelt gratitude to IISEE, BRI, GRIPS, and JICA for granting me the opportunity to participate in this training course. My deepest appreciation goes to my supervisor, Dr. Eri Ito, for her invaluable guidance and support, which were essential to the successful completion of this research. I am also thankful to all those who contributed to the data collection through the SATREPS Project activities.

REFERENCES

Álvarez-Gómez, J. A., Aniel-Quiroga, Í., Gutiérrez-Gutiérrez, O. Q., Larreynaga, J., González, M., Castro, M.,…Carreño, E. (2013). Natural Hazards and Earth System Sciences, 13(11), 2927-2939.

Bommer, J. J., Benito, M., Ciudad-Real, M., Lemoine, A., López-Menjívar, M., Madariaga, R.,…Nieto-Lovo, M. (2002). Soil dynamics and earthquake engineering, 22(5), 389-418.

Canora, C., Martínez-Díaz, J. J., Villamor, P., Berryman, K., Álvarez-Gómez, J. A., Pullinger, C., & Capote, R. (2010). Bulletin of the Seismological Society of America, 100(6), 2873-2890.

DeMets, C., Gordon, R. G., & Argus, D. F. (2010). Geophysical journal international, 181(1), 1-80.

Fernández A, M. (2011). Revista geológica de América central, 26. https://doi.org/10.15517/rgac.v0i26.8532

Guzmán‐Speziale, M., Pennington, W. D., & Matumoto, T. (1989). Tectonics, 8(5), 981-997.

Ito, E., Nakano, K., Nagashima, F., & Kawase, H. (2020). Bulletin of the Seismological Society of America, 110(6), 2892-2911.

Kawase, H., Mori, Y., & Nagashima, F. (2018). Earth, Planets and Space, 70, 1-32.

Kawase, H., Sánchez-Sesma, F. J., & Matsushima, S. (2011). Bulletin of the Seismological Society of America, 101(5), 2001-2014.

Martínez-Díaz, J. J., Álvarez-Gómez, J. A., Staller, A., Alonso-Henar, J., Canora, C., Insúa-Arévalo, J. M.,…Hernández-Moreno, C. (2021). Journal of South American Earth Sciences, 105, 103038.

Matsushima, S., Hirokawa, T., De Martin, F., Kawase, H., & Sánchez‐Sesma, F. J. (2014). Bulletin of the Seismological Society of America, 104(1), 381-393. https://doi.org/10.1785/0120120321

Nagashima, F., Kawase, H., & Matsushima, S. (2017). 16th World Conference on Earthquake, 16WCEE,

Nagashima, F., Matsushima, S., Kawase, H., Sánchez‐Sesma, F. J., Hayakawa, T., Satoh, T., & Oshima, M. (2014). Bulletin of the Seismological Society of America, 104(5), 2288-2302.

Nakamura, Y. (1989). Railway Technical Research Institute, Quarterly Reports, 30(1).

Sánchez-Sesma, F. J., Rodríguez, M., Iturrarán-Viveros, U., Luzón, F., Campillo, M., Margerin, L.,…Rodríguez-Castellanos, A. (2011). Geophysical Journal International, 186(1), 221-225. https://doi.org/10.1111/j.1365-246X.2011.05064.x

Yamanaka, H. (2007). 物理探査, 60(3), 265-275.